Examples of the use of anemometry and flow visualisation for experimental studies of physical speech production mechanisms

Annemie van Hirtum

HAL Id: hal-00692420
https://hal.science/hal-00692420

Submitted on 30 Apr 2012

ACOUSTICS 2012

Examples of the use of anemometry and flow visualisation for experimental studies of physical speech production mechanisms

A. Van Hirtum

Gipsa-lab, UMR CNRS 5126, Grenoble Universities, 38000 Grenoble, France
annemie.vanhirtum@gipsa-lab.grenoble-inp.fr

A qualitative and quantitative study of flow variables is a main ingredient of physical studies of human speech production. Nevertheless, the term 'human speech sounds' stands for a large variety of sounds which are produced using different mechanisms and which can be roughly divided into two categories: voiced and unvoiced sounds. Voiced sounds are due to a fluid structure interaction in the glottis between airflow coming from the lungs and the surrounding deformable vocal folds tissues. Unvoiced sounds on the other hand are due to the interaction of a turbulent jet issued somewhere in the upper airways and a quasi rigid obstacle such as tongue or teeth. As such physical modelling of voiced sounds requires qualitative and quantitative knowledge of the mean flow properties and the tissue properties in order to estimate the force distribution on the vocal folds tissues. The study of unvoiced sounds on the other hand requires besides knowledge of the mean flow the qualitative and quantitative characterisation of the fluctuating flow field. Consequently, in case unvoiced sounds are of interest the combined use of flow visualisation and anemometry becomes highly attractive since fluctuations due to vortex generation and/or randomness can be studied qualitatively as well as quantitatively.

1 Introduction

There is significant interest in low and moderate speed jets within the context of naturally occurring jets as is the case for human speech sound production. Indeed, the Reynolds numbers associated with human speech sound production are $Re_b < 10^4$ so that low and moderate speed jet formation occurs at a constriction along the vocal tract (e.g. at the glottis during voiced sound production or downstream from the teeth during fricative sibilant sound production). In addition, it is well accepted to make severe simplifications of the geometry of interest, so that the vocal tracts geometry is commonly represented as a rigid circular tube or a rectangular channel [2, 15]. Consequently, in case a circular tube is used a round jet is formed. Despite numerous experimental and numerical studies of plane jets, most research focus on high Reynolds number flow ($Re_b > 10^4$) and well designed nozzles due to their importance for technological applications. As a consequence, several authors report the lack of data in relation to jets at low or moderate Reynolds numbers in general [8, 13] or in relation to biofluid mechanics such as human speech production [11]. The current study aims to contribute to the understanding of flow development and generation of coherent structures in the mixing layer of the round jet for low to moderate Reynolds numbers by considering a systematic study as function of Reynolds number in the range $10^3 < Re_b < 1.2 \times 10^4$ for a circular uniform pipe nozzle downstream from a sharp edged abrupt contraction.

2 Experimental setup

2.1 Channel flow facility

A schematic diagram of the experimental setup is shown in Fig. 1. The facility consists of an air compressor [a] (Atlas Copco GA7), followed by a pressure regulator [b] (Norgren type 11-818-987) providing an airflow at constant pressure. The volume flow rate is controlled by a secondary manual valve [c] placed downstream the regulator and measured by a thermal mass flow meter (model 4043 TSI) [d] with an accuracy of 2% of its reading. To homogenize the flow, a settling chamber [e] is used with volume 0.25×0.3×0.35 m³ to which a series of 3 perforated plates with holes of diameter 0.0015 m are added. The walls of the settling chamber are tapered with acoustic foam (SE50-AL-ML Elastomeres Solutions) in order to avoid acoustic resonances. Downstream the settling chamber, a uniform extension tube [f] of diameter $D = 25$ mm and varying length L is connected with a
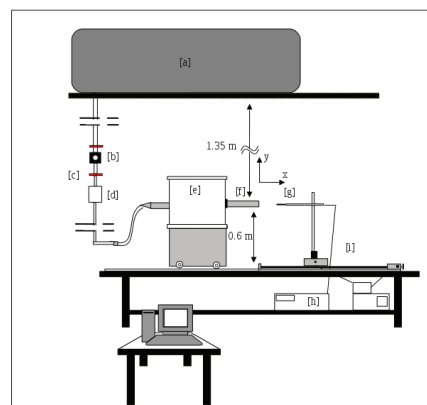

Figure 1: Schematic of the setup [a] air compressor, [b] pressure regulator, [c] valve, [d] volume flow rate, [e] settling chamber, [f] pipe section, [g] hot film, [h] IFA-300 TSI, [i] positioning system.

flat disk to ensure an axisymmetric pipe inlet. Thus the airflow sustains an abrupt area contraction equal to 40:1 from the settling chamber to the pipe. During experiments 2 tube lengths are assessed, $L = 3$ and $L = 133$ cm, corresponding to length-to-diameter ratios $L/D = 1.2$ and $L/D = 53.2$. The imposed volume airflow rates Q are varied from 20 l/min up to 200 l/min by 10 l/min steps, in order to explore bulk Reynolds numbers in the range $10^3 < Re_b < 1.2 \times 10^4$. The bulk Reynolds number Re_b is defined from pipe bulk velocity U_b and pipe diameter D as $Re_b = \frac{U_b D}{\nu} = \frac{4Q}{\nu \pi D}$ with air kinematic viscosity $\nu = 1.5 \times 10^{-5}$ m²/s.

For all experiments, the jet airflow velocity is studied with a hot film (model 1201-20 TSI) [g], having a diameter of 50.8 μm and a working length of 1.02 mm, used in combination with a IFA 300 anemometer (TSI) [h]. All data are collected on a 16 bit A/D data acquistition chard (National Instruments). The hot film is calibrated according to the technique described in [7] which results in a calibration curve fitted on a fourth order polynomial law. The hot film is mounted on a two dimensional stage positioning system (Chuo precision industrial co. CAT-C, ALS-250-C2P and ALS-115-E1P) [i] with accuracy of 4 μm in the streamwise x direction and 2 μm in the transverse y direction. The initial velocity profile at the tube exit is measured along the transverse y direction and the longitudinal centerline velocity profile along the x direction. For the initial transverse velocity profile the hot film is placed downstream, at a distance $x/D \leq 0.04$, from the pipe exit and the applied transverse spatial step

yields $\Delta y = 10^{-4}$ m in the range $-0.7 < y/D < 0.7$. Longitudinal velocity data along the jet centerline are collected along the pipe axis, at $y/D = 0$, from $x/D \leq 0.04$ up to $x/D < 20D$ with a longitudinal spatial step $\Delta x = 10^{-3}$ m.

At each measurement position, velocity data are sampled at 40 kHz during 4 seconds consecutively. Statistical quantities are calculated from instantaneous velocity measurements to which a 10 kHz low pass filter is applied. The local mean velocity $\overline{U}$ and local turbulence intensity T_U,

$$T_U = \frac{\sigma}{\overline{U}} \sigma = \sqrt{\frac{1}{N_{tot}} \sum_{p=1}^{N_{tot}} \left(U_p - \overline{U}\right)^2}, \qquad (1)$$

are quantified with N_{tot} denoting the total number of samples, velocity root mean square σ and U_p the pth instantaneous sample. Uncertainties on mean velocity $\overline{U}$ and turbulence intensity T_U are estimated as <1% for $1.4 < U_p < 10$ m/s and <5% for $0.4 < U_p < 1.4$ m/s [6].

2.2 Flow visualisation

Flow visualization is obtained by smoke injection. Neutrally buoyant white smoke is injected by means of a fog machine (Kool Light, FOG-1200E, 1200W, maximum volume flowrate 300 m^3/min). Two dimensional illumination is applied with a two-dimensional laser light beam. The laser light sheet is generated by a class IIIb laser light source (Laserglow Technologies, LRS-0532-TFM-00200-10, 234.2 mW, wavelength of 532 nm and with spectral linewidth < 0.1 nm) to which a 10 degree cylindrical lens is added. The resulting laser sheet has a thickness <3mm. To record the illuminated smoke pattern, a color camera (Casio, EXILIM Pro EX-F1, 6.0 million effective pixels and 12X optical zoom) is positioned perpendicular to the laser sheet. The back wall of the test chamber is painted in black to ensure a good contrast with the smoke pattern. Movies are recorded at 300 fps so that the time interval between consecutive images is 3.3ms which ensures a good freezing of the flow development.

3 Near field flow visualisation

Instantaneous flow visualisation images of the jet flow for 6 Reynolds numbers Re_b = 1131, 1697, 2263, 2829, 3961, 11317 and length to tube diameter ratios L/D = 1.2 and L/D = 53.2 are illustrated in Fig. 2. The view field extends from the tube exit up to $x \leq 5D$ downstream in order to focus on the near field development.

For the long pipe nozzle, L/D = 53.2, no coherent structures are observed in the near field for Reynolds numbers Re_b = {1131, 1697}. The flow pattern is dominated by a large laminar core. A jet flow instability emerges at Reynolds number Re_b = 2263 in accordance with the helical nature of laminar pipe flow for $L/D > 40$ [5, 9, 16, 1, 3]. A further increase in Reynolds number amplifies the instabilities and leads to an important decrease of the laminar core extent and the appearance of a turbulent region. Large axisymmetrical coherent vortices are not observed. The onset of

(a) $Re_b = 1131, L/D = 1.2$ (b) $Re_b = 1131, L/D = 53.2$

(c) $Re_b = 1697, L/D = 1.2$ (d) $Re_b = 1697, L/D = 53.2$

(e) $Re_b = 2263, L/D = 1.2$ (f) $Re_b = 2263, L/D = 53.2$

(g) $Re_b = 2829, L/D = 1.2$ (h) $Re_b = 2829, L/D = 53.2$

(i) $Re_b = 3961, L/D = 1.2$ (j) $Re_b = 3961, L/D = 53.2$

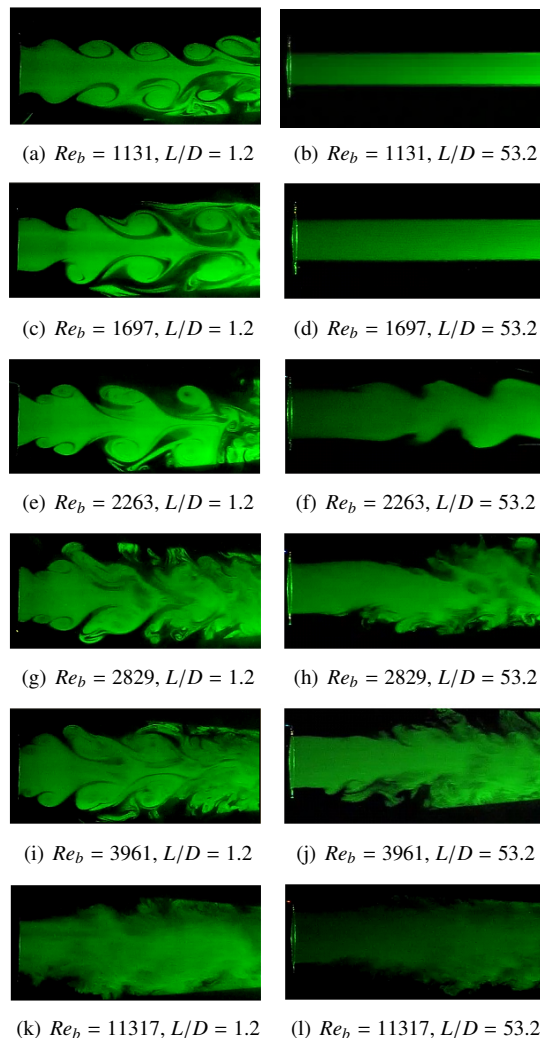(k) $Re_b = 11317, L/D = 1.2$ (l) $Re_b = 11317, L/D = 53.2$

Figure 2: Near field flow images ($0 \leq x/D \leq 5$).

instabilities in the range $2000 < Re_b < 3000$ is in accordance with observations of pipe flow issuing from a smooth long pipe nozzle in case a large disturbance is introduced at the inlet [17, 16]. Therefore, the presence of an abrupt contraction at the pipe inlet can be seen as a geometrical disturbance reducing the Reynolds numbers associated with the transition regime compared to transitional Reynolds numbers $Re_b \approx 10^4$ observed for pipe flow in absence of such disturbances [17, 16].

In case of a short nozzle $L/D = 1.2$, images clearly illustrate the dependence of the flow structure on Reynolds number. For the lowest Reynolds numbers $Re_b = 1131$, the vorticity layer immediately downstream the nozzle exit rolls up so that axisymmetric large scale structures are formed surrounding the potential core and engulfing both ambient and pure jet fluid. Large ring vortices with an elliptic form are generated for which the main axis remains parallel to the main flow direction and the vortices reach the centerline after growing by moving downstream. Consequently, the interaction of large scale structures and their deformation in the near field is limited so that the centerline velocity at the tube outlet is expected to be only weakly imprinted by the vortex presence. The presence of the abrupt contraction triggers the shear layer roll up at the nozzle exit so that generation of ring vortices is shifted upstream compared to a smooth contraction nozzle [14].

For $Re_b = \{1697, 2263, 2829\}$, the vortex size increases and a smaller tailing vortex is observed immediately behind the large leading vortex at $x/D \approx 1$. The collapse of the two vortices at $x/D \approx 2$ into a single one suggests a vortex pairing process to take place at a spatial position observed for transitional jet flow at high Reynolds numbers $Re_b > 10^4$ as described by the two ring model for the axisymmetric jet issuing from a smooth contraction nozzle [9]. This fusion has for consequence to impulse a deformation in the rotation in the main axis which is likely to affect the velocity along the centerline. In addition, the collapse of the surrounding mixing layer is also more evident compared with $Re_b = 1131$. At $Re_b = 2263$, similar phenomena take place involving larger vortices so that a stronger fluctuation of the centerline velocity is expected.

At $Re_b = 3961$, large scale vortex formation and pairing are still observable. Nevertheless, the structure coherence is less evident than for lower Reynolds numbers. Increasing the Reynolds number beyond $Re_b = 4000$ has for effect to limit the vortex size, and to quickly destroy them. Consequently, for the highest Reynolds numbers, the presence of large structures is not observed, and is replaced by small surrounding structures and turbulent flow behaviour.

4 Temporal analysis

A sequence of the fluctuating velocity signal $U_p(t)/\bar{U}_0$, with physical time t, at 3 downstream positions along the centerline $x/D \leq 0.04$, $x/D = 1$, $x/D = 5$ is shown for Reynolds numbers $Re_b = \{1131, 1697, 2263, 11317\}$ for $L/D = 1.2$ in Fig. 3. For $L/D = 1.2$ and $Re_b = 1131$, the instantaneous centerline velocity is characterised by a quasi periodical fluctuation as the flow moves downstream from $x/D \leq 0.04$ to $x/D = 1$, the fluctuation reduces further downstream as seen at $x/D = 5$. As the Reynolds number increases to $Re_b = 1697, 2263$ a strong regular quasi periodical fluctuation is obtained at $x/D \leq 0.04$. The same way as for $Re_b = 1131$ the fluctuation is amplified at $x/D = 1$ and looses its quasi periodicity at $x/D = 5$. Further increasing of the Reynolds number results in an absence of a quasi periodical fluctuation at all measurement stations as illustrated for $Re_b = 11317$.

So, from Fig. 3 it is seen that a quasi periodic fluctuation of the temporal velocity signal occurs in the downstream region for $L/D = 1.2$ for Reynolds numbers for which large coherent structures are observed in Fig. 2. Consequently, no quasi periodic fluctuations are observed for $Re_b = 11317$. Moreover, the fluctuation amplifies for Reynolds numbers in the transitional regime, $1132 < Re_b \leq 4527$ corresponding to a peak in initial turbulence. The measurement station situated just downstream the potential core extent at $x/D = 5$, since $x_{pc}/D \leq 4$ holds for $L/D = 1.2$, bears only traces of the quasi periodicity since the shear layers collapses outside the potential core so that vortices break down rapidly and turbulence is created. Flow visualisation results as shown in Fig. 2 suggest that the amplification of the quasi periodic fluctuation between $x/D \leq 0.04$ and $x/D = 1$ as well as the amplification with Reynolds number is due to growing of unstable vortices nearest to the centerline so that the transverse extent

of the jets central core decreases and the centerline velocity becomes more affected by the passing and interaction of vortices. For $Re_b = 1131$ the Reynolds number is sufficiently low so that the jet shear layer structures are only marginaly unstable which limits their growth [1, 5]. Consequently, the hump in streamwise turbulence intensity before the potential core onset as observed in this study for $L/D = 1.2$ in Fig. **??** and reported for a contraction jet in among others [14, 12, 4] is indeed due to the passage of unstable large scale coherent structures and not to the creation of real small scale and random velocity fluctuations. The coherent structures observed for the lowest Reynolds number $Re_b = 1131$ are stable and hence no hump in centerline turbulence can be observed.
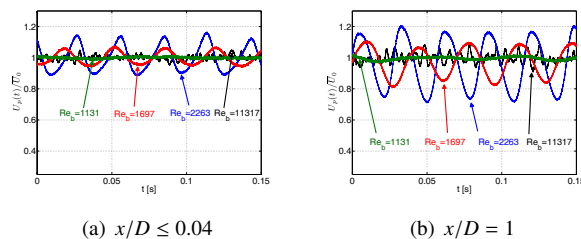

(a) $x/D \leq 0.04$ (b) $x/D = 1$

Figure 3: $U_p(t)/\bar{U}_0$ for $L/D = 1.2$ and $Re_b = \{1131, 1697, 2263, 11317\}$.

For $L/D = 53.2$ no quasi periodical fluctuation is observed for $Re_b = 1131$ and $Re_b = 11317$ whereas a slow fluctuation occurs for $Re_b = 2263$. For $L/D = 53.2$ no coherent structures are observed in the jet shear layer visualised in Fig. 2 for $Re_b \leq 1697$ so that no quasi periodic fluctuation is observed for $Re_b = 1131$. For $Re_b = 2263$ a helical coherent structure is observed resulting in a low frequency quasi periodic fluctuation. The same way as for $L/D = 1.2$ increasing the Reynolds number will eventually lead to limit the vortex size so that vortices are quickly destroyed and no quasi periodic fluctuations can be observed as illustrated for $Re_b = 11317$.

5 Spectral analysis

A spectral analysis of the instantaneous velocity is assessed for $L/D = 1.2$ and $L/D = 53.2$. Strouhal numbers are derived from the bulk velocity and the tube diameter D denoted $St_D = \frac{fD}{U_b}$ and from the bulk velocity and momentum thickness denoted $St_{\delta^{**}} = \frac{f\delta^{**}}{U_b}$. The power spectral density of the velocity signal in the near field for measurement stations along the centerline at $x/D = 1$, $x/D = 2$, $x/D = 3$, $x/D = 4$ and $x/D = 5$ is presented as function of Reynolds number, $Re_b = \{1131, 1697, 2263, 2829, 3961, 11317\}$, for $L/D = 1.2$ in Fig. 4 and for $L/D = 53.2$ in Fig. 5. Each spectrum is shifted downwards with respect to the previous.

From Fig. 4, it is seen that the spectra obtained for $L/D = 1.2$ are characterised by broad and/or sharp frequency peaks for which the spectral position and amplitude vary as function of Reynolds number Re_b and measurement station x/D. For $L/D = 1.2$ and Reynolds number $Re_b = 1131$, the spectra exhibit a broad frequency peak at approximately 14 Hz, corresponding to Strouhal number $St_D \approx 0.55$ for all measurement stations $1 \leq x/D \leq 5$. The amplitude of the broad
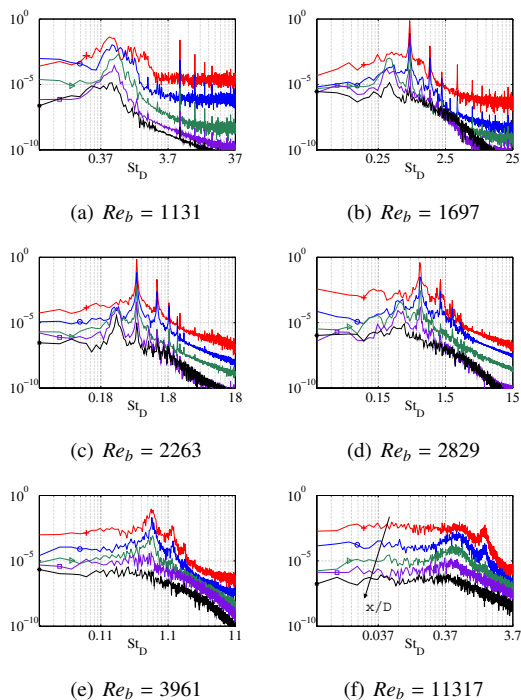
(a) $Re_b = 1131$

(b) $Re_b = 1697$

(c) $Re_b = 2263$

(d) $Re_b = 2829$

(e) $Re_b = 3961$

(f) $Re_b = 11317$

Figure 4: Centreline velocity spectra for $L/D = 1.2$ at positions $x/D = 1$ (+), $x/D = 2$ (∘), $x/D = 3$ (▷), $x/D = 4$ (□), $x/D = 5$ (∗). x/D increases as indicated by the arrow in Fig. 4(f). Every spectrum is shifted downwards.

peak amplifies as x/D increases to $x/D = 3$ and reduces at $x/D = 5$. The broad peak is associated with the roll up of the initial vorticity sheet into a toroidal vortex ring. The maintenance of the peak, regardless x/D, confirms the quasi stability of coherent structures for $Re_b = 1131$ as observed from flow visualisation in Fig. 2 as from the temporal velocity signal. For $Re_b = 1697$, a sharp peak at 30 Hz appears comparable to those observed in the jet shear layer. In addition, harmonics are observed at $x/D = 1$ and $x/D = 2$. The presence of this sharp energy peaks in the centerline power spectrum confirms the formation of vortices and the convection of surrounding vortices at specific frequencies. A broad subharmonic emerges at approximately 15 Hz at $x/D \geq 3$ along with a reduced amplitude of the sharp energy peak and the disappearance of the harmonics. The appearance of the subharmonic is associated with the pairing of two ring vortices illustrated in Fig. 2. The general tendencies outlined for $Re_b = 1697$ are also observed for $2263 \leq Re_b \leq 3961$. The frequency of the peaks shifts to higher frequencies as the Reynolds number increases corresponding to an acceleration in the vortex generation resulting in increased instability and interaction of the coherent structures so that the amplitude of the peaks varies with Reynolds number. For $Re_b = 2263$ the amplitude of the peaks increases due to the reduced central jet portion so that the centerline velocity is most influenced by the passing of coherent structures and their interaction. For $2263 < Re_b \leq 3961$ the amplitude of the peaks, sharp as well as broad, gradually decreases so that for $Re_b = 2829$ the velocity spectrum is flattened out at $x/D = 5$. For $Re_b = 3961$ the spectra are flattened out at $x/D = 4$ and $x/D = 5$ resulting in spectra characteristic for turbulent flow. Finally, for $Re_b = 11317$ all spectra are flattened out, so that no well defined sharp peaks are observed.

Power spectra along the centerline for $L/D = 53.2$ (Fig. 5) are not characterised by sharp energy peaks. Instead for $Re_b = 1131$ a broad low frequency peak appears at approximately 6 Hz. The amplitude of the peak increases as the Reynolds number increases from $Re_b = 1131$ to $Re_b = 2263$ in agreement with the low frequency quasi periodic fluctuation observed in the temporal signal and the visualisation of helical vortices for $Re_b = 2263$ shown in Fig. 2. A further increase of Reynolds number flattens the power spectra so that broadband spectra are obtained for all measurement stations x/D for $Re_b \geq 3961$. For $L/D = 53.2$, the normalised boundary layer thickness δ_{95}/D yields values greater than those observed for $L/D = 1.2$. As a consequence, the jet shear layer is more difficult to disturb and no toroidal ring vortices are generated.
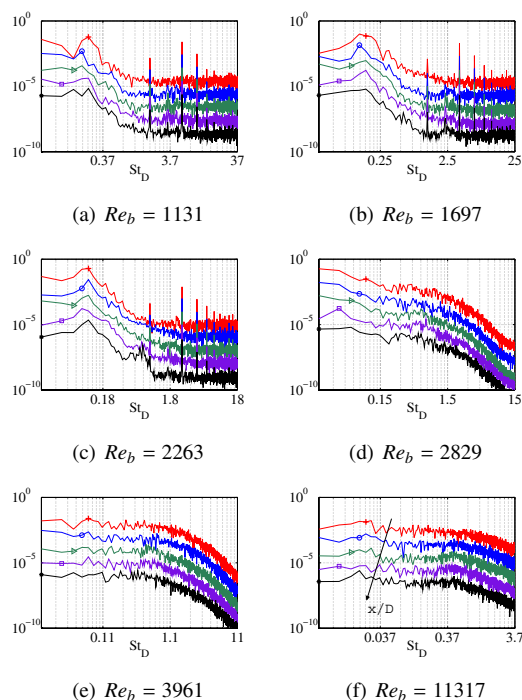

(a) $Re_b = 1131$

(b) $Re_b = 1697$

(c) $Re_b = 2263$

(d) $Re_b = 2829$

(e) $Re_b = 3961$

(f) $Re_b = 11317$

Figure 5: Centerline velocity spectra for $L/D = 53.2$ at five downstream positions $x/D = 1$ (+), $x/D = 2$ (∘), $x/D = 3$ (▷), $x/D = 4$ (□), $x/D = 5$ (∗). x/D increases as indicated by the arrow in Fig. 5(f). Every spectrum is shifted downwards.

Table 1 presents an overview of Strouhal numbers St_D characterising the centerline spectra shown in Fig. 4 for $L/D = 1.2$ and in Fig. 5 for $L/D = 53.2$. The Strouhal number St_D is shown in order to compare with values reported for a smooth contraction nozzle given in [14]. Two peak values are reported on. The main frequency associated with vortex formation and the frequency after vortex pairing. The uncertainty on the reported values is due to low spectral resolution for low frequencies and to the variation of the peak frequency as the spatial measurement position is shifted downstream from $x/D = 1$ to $x/D = 5$.

For $L/D = 53.2$, St_D peaks are associated with main vortex formation since no vortex pairing is observed. The non dimensional frequencies St_D decreases as the Reynolds number increases from $St_D \approx 0.18$ to $St_D \approx 0.10$. Non dimensional frequencies associated with main vortex formation for $L/D = 1.2$ show the same Reynolds dependence since a de-

	$L/D = 1.2$		$L/D = 53.2$	
Re_b	pairing	formation	pairing	formation
1131	-	0.6 ± 0.1	-	0.18 ± 0.05
1697	0.38 ± 0.05	0.71 ± 0.01	-	0.12 ± 0.03
2263	0.32 ± 0.01	0.63 ± 0.01	-	0.10 ± 0.01
2829	0.32 ± 0.01	0.61 ± 0.01	-	-
3961	-	0.60 ± 0.01	-	-

Table 1: $St_D(Re_b, L/D)$ for vortex pairing and formation.

crease from $St_D \approx 0.7$ down to $St_D \approx 0.6$ is found. Consequently, Strouhal numbers St_D associated with $L/D = 1.2$ are a multiple of Strouhal numbers St_D for $L/D = 53.2$. The ratio $St_D(L/D = 1.2)/St_D(L/D = 53.2)$ increases from ≈ 3 for $Re_b = 1131$ to ≈ 6 for $Re_b = 2263$. The multiplication factor for low Reynolds numbers is partly explained by the difference in initial momentum thickness δ^{**}. Indeed, Fig. **??** shows that for $Re_b < 3000$ the momentum thickness for $L/D = 53.2$ yields approximately three times values observed for $L/D = 1.2$. Therefore, for $Re_b = 1131$ the Strouhal number based on the momentum thickness yields $St_{\delta^{**}} \approx 0.01$ for both L/D ratios. As the Reynolds number increases the Strouhal number based on the momentum thickness for $L/D = 1.2$ remains $St_{\delta^{**}} \approx 0.01$, which is in accordance with the order of magnitude of $St_{\delta^{**}}$ reported in [9] for transitional round jet flow at $Re_b = 15 \times 10^4$, whereas for $L/D = 53.2$ its value decreases. Consequently, the Reynolds dependence of vortex formation for $L/D = 53.2$ is more pronounced than for $L/D = 1.2$.

For $L/D = 1.2$, Strouhal numbers St_D associated with vortex formation $0.6 < St_D < 0.71$, reported in Table 1, are higher than values $0.5 < St_D < 0.6$ reported in [14] for a smooth contraction nozzle. Since the boundary layer thickness at the tube exit yields $\delta_{95} \approx 0.1D$ in the current study as well as in [14] the found increase for the current study is due to the presence of sharp edges at the contraction inlet. In addition, found St_D values in the current study reduces with Reynolds number whereas values reported in [14, 10] show the opposite tendency. This finding suggests that the influence of the upstream sharp edges on vortex formation decreases as the Reynolds number increases so that $St_D \approx 0.6$ for $Re_b \approx 4000$ in the current study as in well as in values reported in [14].

From Table 1, it is seen that in case of $L/D = 1.2$ non dimensional frequencies St_D associated with paired vortices yield half of values associated with vortex formation at the same Reynolds number, as expected for a subharmonic. The same observation is made in [14]. The retrieved values $St_D \approx 0.3$ correspond to the natural frequency observed for higher Reynolds number forced jets [4]. In general, spectra observed for $L/D = 1.2$ in the transitional regime $1131 < Re_b < 4000$ are shaped by vortex formation, appearance of harmonics, vortex pairing and finally vortex breakdown and entrainment. This description is in accordance with the two ring model for a transitional axisymmetrical jet at high Reynolds number $Re_b = 15 \times 10^4$ outlined in [9].

6 Conclusion

Jet dynamics downstream from an abrupt contraction with sharp edges coupled to a uniform circular tube extension with length to diameter ratio $L/D = 1.2$ and $L/D = 53.2$ is studied as function of moderate Reynolds numbers in the range $1131 < Re_b < 11320$ by flow visualisation and hot film anemometry. The presence of an abrupt contraction at the nozzle inlet disturbs the flow so that the jet becomes transitional for low Reynolds numbers in the range $1131 < Re_b < 4000$ for both assessed length to diameter ratios. As a consequence, the near field behaviour is dominated by the generation, passage and interaction of large flow structures.

References

[1] P. 0'Neill, J. Soria, and D. Honnery. The stability of low Reynolds number round jets. *Exp. Fluids*, 36:473–483, 2004.

[2] J. Cisonni, A. Van Hirtum, X. Pelorson, and J. Willems. Theoretical simulation and experimental validation of inverse quasi one-dimensional steady and unsteady glottal flow models. *J. Acoust. Soc. Am.*, 124:535–545, 2008.

[3] J. Cohen and I. Wygnanski. The evolution of instabilities in the axisymmetric jet. part 1. The linear growth of disturbances near the nozzle. *J. Fluid Mech.*, 176:191–219, 1987.

[4] S.C. Crow and F.H. Champagne. Orderly structure in jet turbulence. *J. Fluid Mech.*, 48:547–591, 1971.

[5] P.E. Dimotakis, R.C. Miake-Lye, and D.A. Papantoniou. Structure and dynamics of round turbulent jets. *Phys. Fluids*, 23:3185–3192, 1983.

[6] X. Grandchamp. *Modélisation physique des écoulements turbulents appliquée aux voies aériennes supérieures chez l'humain*. PhD thesis, Grenoble University, 2009.

[7] X. Grandchamp, A. Van Hirtum, and X. Pelorson. Hot film/wire calibration for low to moderate flow velocities. *Meas. Sci. Technol.*, 21:115402, 2010.

[8] F.F. Grinstein. Vortex dynamics and entrainment in rectangular free jets. *J. Fluid Mech.*, 437:69–101, 2001.

[9] F.F. Grinstein, M.N. Glauser, and W.K. George. *Fluid vortices*, chapter Vorticity in jets, pages 65–94. Kluwer Academic Publisher, New York, 1995.

[10] C. Ho and P. Huerre. Perturbed free shear layers. *Annu. Rev. Fluid Mech.*, 16:365–424, 1984.

[11] M. Howe and R. McGowan. Aeroacoustics of [s]. *Proc. Roy. Soc. A*, 461:1005–1028, 2005.

[12] J. Mi, D. Nobes, and G. Nathan. Influence of jet exit conditions on the passive scalar field of an axisymmetric free jet. *J. Fluid Mech.*, 432:91–125, 2001.

[13] M.E. Schneider and R.J. Goldstein. Laser Doppler measurement of turbulence parameters in a two-dimensional plane wall jet. *Phys. Fluids*, 6:3116–3129, 1994.

[14] V. Todde, P.G. Spazzini, and M. Sandberg. Experimental analysis of low-Reynolds number free jets: Evolution along the jet centerline and Reynolds number effects. *Exp. Fluids*, 47:279–294, 2009.

[15] A. Van Hirtum, X. Pelorson, O. Estienne, and H. Bailliet. Experimental validation of flow models for a rigid vocal tract replica. *J. Acoust. Soc. Am.*, 130:2128–2138, 2011.

[16] I. Wygnanski, M. Sokolov, and D. Friedman. On transition in a pipe: Part 2. The equilibrium puff. *J. Fluid Mech.*, 69:283–304, 1975.

[17] I.J. Wygnanski and F.H. Champagne. On transition in a pipe: Part 1. The origin of puffs and slugs and the flow in a turbulent slug. *J. Fluid Mech.*, 59:281–335, 1973.